Formation and Decomposition of Ethane, Propane, and Carbon Dioxide Hydrates in Silica Gel Mesopores under High Pressure

E. Ya. Aladko,[‡] Yu. A. Dyadin,[†,‡] V. B. Fenelonov,[§] E. G. Larionov,[‡] A. Yu. Manakov,*[,‡] M. S. Mel'gunov,[§] and F. V. Zhurko[‡]

Nikolaev Institute of Inorganic Chemistry, SB RAS, Lavrentyev Avenue 3, Novosibirsk 630090, Russia, and Boreskov Institute of Catalysis, SB RAS, Lavrentyev Avenue 5, Novosibirsk 630090, Russia

Received: April 16, 2006; In Final Form: July 10, 2006

The experimental data on decomposition temperatures for the gas hydrates of ethane, propane, and carbon dioxide dispersed in silica gel mesopores are reported. The studies were performed at pressures up to 1 GPa. It is shown that the experimental dependence of hydrate decomposition temperature on the size of pores that limit the size of hydrate particles can be described on the basis of the Gibbs−Thomson equation only if one takes into account changes in the shape coefficient that is present in the equation; in turn, the value of this coefficient depends on a method of mesopore size determination. A mechanism of hydrate formation in mesoporous medium is proposed. Experimental data providing evidence of the possibility of the formation of hydrate compounds in hydrophobic matrixes under high pressure are reported. Decomposition temperature of those hydrate compounds is higher than that for the bulk hydrates of the corresponding gases.

Introduction

Confined porous space of a host rock can result in a change of gas hydrate decomposition temperature, T and pressure P. The main reason of this change is physical limitation of the growth of guest hydrate particles inside a host pore by its walls. For example, in coarsely dispersed rocks such as gritstone, the temperature of hydrate decomposition is equal to the temperature of decomposition, T_0, of a macroscopic bulk phase. But in more dispersed media, T is usually lower than T_0, and the equilibrium pressure of dissociation, P, exceeds P_0, where P_0 is the pressure of dissociation of the macroscopic bulk phase.[1−8] The structure, dynamics, and thermodynamic properties of confined species (will be denoted as guest or G) depend on many factors such as confining geometry, physical and chemical properties of the confining surface, interaction at interfaces, the real composition of surrounding water, properties of a liquid-phase film between the hydrate and the porous media (will be denoted as host H), and so on, and the effect of each factor is in many respects yet little understood.[3,4,9,10]

The phenomenon of the dependence of phase transformation temperature on size manifests, for example, in melting of metallic,[11−13] organic,[14,15] or semiconducting[16] nanoparticles, the freezing/melting of water,[9,10,17−19] and other liquids of various complexity[9,10,20] including ionic ones[21] confined in nanospace, i.e., this phenomenon is universal. It was predicted at the end of 19th century[22] by J. J. Tomson, who explained it using the fundamental Clausius−Clapeyron equation, but he did not offer a formulated equation. According to our knowledge, the first qualitative relationships were introduced by Pawlow[23] and Rie,[24] and later this problem was discussed extensively by Batchlor and Foster,[25] Defay, Prigogine, et al.,[26] and others, e.g., refs 12, 14, 27, 28. The last and the most exact asymptotic equation in classic thermodynamic approximation for any bulk first-order phase transition was proposed presumably by Evans and Marini Bettolo Marconi.[29,30] Quinson et al.[31−33] developed a new method of measuring of pore size distributions, called thermoporometry, which is based on the measurement of the freezing temperature decrease (ΔT) for a fluid confined in the nanopores. The basics of thermoporometry is discussed, e.g., at refs 34, 35.

During the past decades, this field has being studied intensively by modern theoretical and precise experimental methods applying state-of-the-art instruments. The majority of theoretical studies are based on the density functional theory for statistical mechanics (DFT), molecular dynamics (MD), Monte Carlo (MC), and other computational methods; the most recent works are discussed in ref 10 (see also, e.g., refs 9, 36).

According to known publications in this field, one can conclude that the most general reason of size effects is in the excess of surface energy of the atoms or molecules on the guest interface compared to that for atoms in the bulk. The excess surface energy can be compensated via the interaction with atoms of the surrounding medium.[10,27,30] The most widespread situations correspond to weak guest−host interactions, when the excess energy of surface atoms results in the decrease of phase transformation temperature, although strong guest−host interactions can result in the opposite effect.[10] For example, Kaneko et al. reported detectable *increases* in the freezing temperature caused by strong interaction between benzene or carbon tetrachloride with nanoporous activated carbon.[37,38] Later this was confirmed by Sliwanska-Barkowiak et al.[39] Other examples can be found elsewhere.[9,10]

There is a number of models for quantitative explanation of the dependence of melting point and the temperatures of other phase transformations on size.[2−16,18−30,40] The molecular-statistical simulation methods (DFT, MD, MC, etc.) try to do it on a microscopic (atomic) level, and usual thermodynamic approximations do it on macroscopic level. Both approaches complement each other, and relatively simple analytical equa-

* Corresponding author. E-mail: manakov@che.nsk.su. Telephone: (7-383) 339 13 46. Fax: (7-383) 330 94 89.
† Deceased.
‡ Nikolaev Institute of Inorganic Chemistry.
§ Boreskov Institute of Catalysis.

10.1021/jp062343a CCC: $33.50
Published on Web 09/14/2006

tions can be assumed as approximations of more precision, but difficult for direct accounting computational dependencies. The modern thermodynamic equations are obtained either by accounting the free energies of the confined liquid and solid[41] or by determining the temperature at which the chemical potential of the confined solid becomes equal to that for the bulk solid;[29,30] other theories emphasize the role of the defects and interface interaction,[42−44] etc. Two main pore geometries are usually applied: slits and cylinder. The obtained solutions usually give the thermodynamic equation, which very often is referred to as the Gibbs−Thomson equation:

$$\Delta T_d/T_0 = [(\nu_S\gamma_{SH} - \nu_l\gamma_{LH})/\Delta H_f]\ (\alpha/d) \qquad (1)$$

where $\Delta T_d = T_0 - T_d$, and T_d and T_0 are the transformation temperatures for particles size of d and correspondingly for the bulk phase of the same composition; γ_{SH} and γ_{LH} are the surface energies of "solid G−H" and "liquid G−H" interface, correspondingly; ν_S and ν_L are the molar volumes of solid and liquid G, correspondingly; ΔH_f is the enthalpy of phase transformation, α is the shape coefficient, which values depend on the determination of the characteristic size d. The analysis of the interrelation between α and d is one from the key objects for this topic.

The most widespread solutions of the melting/freezing problem account for the Clausius−Clapeyron equation, which gives the vapor pressure as a function of temperature, and the Kelvin equation, which correlates this vapor pressure with the curvature of a "solid−liquid" interface.[9] For such assumptions, α/d in eq 1 is determined as:

$$\alpha/d = C_c = 2/r_m = (1/R_1 + 1/R_2) \qquad (2)$$

where C_c is the mean curvature of surface, r_m is the mean curvature radius**,** R_1 and R_2 are the principal radii of curvature at a concerned point at a curved surface.[1] [For spherical menisci, $R_1 = R_2 = R_{sph}$ and $\alpha/d = 4/D_{sph}$, where $D_{sph} = 2R_{sph}$ are the diameter and radius of sphere, correspondingly; for cylindrical menisci, $R_1 = R_{Cyl}$ and $R_2 = \infty$, so $\alpha/d = 2/D_{Cyl}$, where $D_{Cyl} = 2R_{Cyl}$ are the diameter and radius of cylinder, correspondingly. It is significant that G has spherical menisci in cylindrical pores and cylindrical menisci in slitlike pores.]

For further consideration one can apply the Young equation:

$$\gamma_{SH} - \gamma_{LH} = \gamma_{SL}\cos\theta \qquad (3)$$

where γ_{SL} is the surface energy of the "solid−host" interface and θ is the contact angle at the "liquid−host" interface. With the assumptions that the change of molar volume at T_d is negligibly small ($\nu_S \approx \nu_L$), $\Delta H_f \approx$ const, and $\cos\theta = 1$ (full wetting), one can rewrite eq 1 in the form:

$$\Delta T_d/T_0 = [\nu_S\gamma_{SL}/\Delta H_f](\alpha/d) = K\,(\alpha/d) \qquad (4)$$

where $K \approx$ const and $\alpha/d = C_c$. This means that the curvature of the "solid−liquid" interface is a key factor.

From our point of view, the most thorough thermodynamic approximation as well as the basics of modern molecular-statistical simulation of the phase equilibrium of the fluids confined in narrow pores are given by Evans et al.[29,30,45] They illustrate eq 1's thorough calculation of the grand potentials of G as the sum of bulk and surface contributions (the interaction on the "G−H" interface) for the slit and cylindrical pores. In the former case, G is confined between two parallel solid walls of H (see Figure 1a); such slits have of infinite area, A, but are separated by a finite distance $d = 2V/A$, where V is the inner

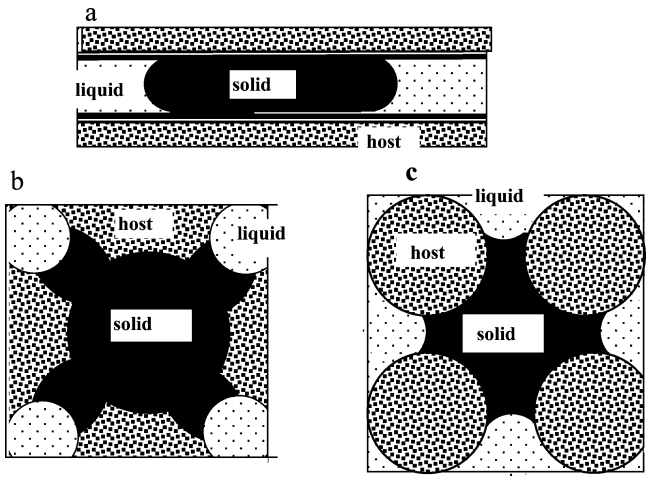

Figure 1. Simplest models of the confined guest location in porous space of host: (a) slit or cylindrical pore, (b) the typical pore for porous glass (the model of spongelike porous solid), (c) the typical pore for silica gel (the corpuscular porous solid model).

infinite volume of this pore. In this case, the ratio α/d in eq 1 is formulated as $2/d$.[29,30] Similarly, analysis of situation of G, confined in a circular straight cylinder with infinite length (see the same Figure 1a, but in this case, the cylindrical pore is assumed). The ratio α/d in eq 1 for cylinder pores is $4/d$, where d is the diameter of cylinder $d_{Cyl} = 4V/A$, the V and A are the inner volume and surface area of this cylinder.

Assumption of the pore infiniteness neglects the influence of so-called edge effects. It is significant that, (i) for such an assumption, the key factor is the situation on a "G−H" interface, and (ii) the relation is true that

$$\alpha/d = A/V \qquad (5)$$

where A/V is the *surface-to-volume ratio*.

Substitution of eq 5 in eq 1 under $\nu_S \approx \nu_l = \nu$ gives

$$\Delta T_d/T_0 = [A(\gamma_{SH} - \gamma_{LH})]/[V(\Delta H_f/\nu)] \qquad (6)$$

where the numerator on the right-hand side $A(\gamma_{SH} - \gamma_{LH}) = A\Delta\gamma = \Delta G_A$. It defines the contribution of the surface energy change caused by replacement of "liquid−host" interface with "solid−host" interface, and denominator $V(\Delta H_f/\nu) = \Delta G_V$ characterizes the contribution of the changes in the bulk during phase transformation. Thus, eq 6 can be rewritten as:

$$\Delta T_d/T_0 = \Delta G_A/\Delta G_V \qquad (7)$$

i.e., the values of $\Delta T_d/T_0$ are determined as the relationship between the events on the guest−host interface and events inside the guest volume. Noteworthy, recording eq 1 in a form of eq 4 makes this relationship almost unclear.

Thus we have two equivalent approaches to describe the problem. One mainly focuses on the phenomena at the "solid−liquid" (only G) interface, another assumes the state at the "G−H" interface as a controlling factor. Unfortunately, this equivalence is true only for the simplest models of constant cross section, when the area of "solid−liquid" interface A_{SL} = const, and any shift of meniscus at this interface results in exact compensation of the change of "solid−H" area ΔA_{SH} with the change of "liquid−H" interface area ΔA_{LH}. Only under this assumption:

$$\alpha/d = A/V = C_c \qquad (8)$$

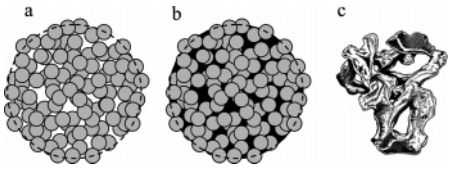

Figure 2. Scheme of silica gel structure without guest (a) and with introduced guest (b), guest shown black; a possible structure of guest (c), host not shown.

where menisci in slitlike pores have semicylinder, while menisci in cylinder-like pores have a semispherical form.

The transition to the models of variable cross section, which have convergent and divergent sections and variable form, brakes the condition of $A_{SL} = \text{const}$, thus in general case $C_c \neq A/V$. For example, parts b and c of Figure 1 show the simple situations, characteristic of porous structures of porous glasses (b) and silica gels (c). Let us consider the equality of the mean curvature of surface of all menisci at the "liquid−solid" interface for all cases shown in Figure 1, i.e. $C_c = 2/r_m$. The additional illustration is shown in Figure 2, where schemes of silica gel structure without guest (a), with introduced guest (b), and only guest (c) demonstrate possible actual situations. Thus, what is the characteristic size of the solid-phase one should assume in these situations if $C_c \neq A/V$?

To answer, one can make computations for the selected species of different specific individual microscopic elements of porous systems, for example, for conelike or wedgelike pores with fixed angles of divergence, etc. But this approach shall not resolve this problem due to the changes of pores shape and their interconnectivity. It is substantial in turn that the large amount of recent simulation and experimental investigations confirm the significance of consideration of the pore shape influence on a confined guest properties.[46−48] Alternative approaches are required, which would bypass the particular values for characterization of the shape and interconnectivity (i.e., *morphological* and *topological* problems[49]).

Let us start from a situation at the "solid−liquid" interface. There is pressure gradient, ΔP_L, at this interface, which is determined by the Laplace−Young equation as $\Delta P_L = C_c \gamma_{SL}$. The condition of the mechanical equilibrium requires the equality of the mean curvature C_c of the surface of "liquid−solid" menisci, which is determined by eq 2. The specific profile of the menisci depends of actual shape of a wetting perimeter, which changes with mechanical movement, and infinitely, the menisci shape approaches to "plateau figures". Additional difficulties are related to indirect influence of "G−H" interaction on menisci shape.[50,51] That is why, in a general case, we can only calculate a numerical value of C_c, (e.g., from Kelvin equation), having nothing to say about the surface area of menisci A_{SL}.

Let us consider the situation at the "G−H" interface now. The experimental and theoretical studies of water freezing/melting show that there always is a layer of "bound water" between ice and the wall of the host.[9,10,19,35,52−54] The water in this layer never crystallizes and remains liquidlike or glasslike because the crystalline lattice cannot form from the molecules in the vicinity of surface as a consequence of its local roughness, curvature, local intermolecular interaction, etc.[10,19] Sklari et al.[52] have shown that the freezing temperature of the contacting layers depends on the density of OH groups at the surface of the host. Morishige et al.[53] found that the freezing of such bound water is independent of the pore size, i.e., this is a surface rather than a confinement effect. Such a decrease of the melting point has been observed for boundary layers of cyclohexane and benzene confined in silica gels.[10] Thus, a correction should be made for the Gibbs−Thomson equation, accounting for the bound guest layer having a thickness of t (~1 nm[9,10,19,35]). In general, the properties of this film depend on hydrostatic pressure ΔP_L, i.e., the situations at the "solid−liquid" and at "G−H" interfaces are interconnected. Formally, the ΔP_L effect may be expressed via changes of γ_{SH} values (the inverse influence of the A/V ratio on "solid−liquid" surface curvature may be expressed via changes of $\cos\theta$ assuming $\cos\theta \neq 1.0$). So the uncertainty at the "G−H" interface can be expressed via terms $(\gamma_{SH} - \gamma_{LH})$ or t, which depend on pressure ΔP_L as well as on the heterogeneity of surface shape, etc.

The previous discussion summarizes two ways of definition of the α/d ratio in eqs 1 and 4, both based on different assumptions. The first accounts for assumptions about a situation at the "solid−liquid" interface, e.g., assumption of menisci shape: semispherical shape with mean curvature radius r_m equal to a radius of an inscribed sphere, $\cos\theta = 1.0$, $\gamma_{SL} = \text{const}$. The second involves the assumptions about the situation at the "G−H" interface, e.g., assumption of the difference $(\gamma_{SH} - \gamma_{LH}) = \text{const}$. Both ways are identical for pores of uniform cross section when they are interrelated by the Young equation.

Thus, under definite conditions, it is possible to use the ratio $\alpha/d = A/V$ for estimations of characteristic size d. The surface-to-volume ratio A/V is the important characteristic of any dispersed matter (particle), which characterizes (if the size is big enough) the ratio of the number of surface atoms to the total number of atoms in particle. So, in the general case, the excess surface energy is proportional to A/V.[27]

Such approximation was applied by Qi and Wang,[13] and Guisbiers and Wautelet[55] for expression of the size and shape dependence of the melting temperature T_d of metallic nanoparticles deposited on a substrate. For example, Qi and Wang assumed that:

$$\Delta T_d/T_0 = 6\alpha_{SF}(r/D_V), \tag{9}$$

where r is the atomic radius of metal, D_V is the particle diameter, expressed as the diameter of a sphere of equivalent volume. The shape factor α_{SF} is defined as $\alpha_{SF} = A/A^*$, where A is the real surface area of the nanoparticles of *any shape* and A^* is the surface area of the *spherical* nanoparticles with diameter D_V. The value of $\alpha_{SF} = 1.0$ for spheres and increases with shape angularity and anisotropy. The equation type of eq 9 was successfully applied for the analysis of $\Delta T_d/T_0$ dependence on D_V for melting of Sn, Pb, In, and Bi nanoparticles.[13] Guisbiers and Wautelet used the ratio A/V to determine the shape factors for Al, Mo, and Ta nanoparticles supported on Si.[55] Essentially, a similar approach is used in a new intriguing theory by Sun et al. According to this approach, the melting point oscillations over the whole range of size[56] can be explained.

The relation between the shape factor α_{SF} by[13] and the earlier defined eq 5 can be determined as:

$$A/V = \alpha/d = (A/A^*)(A^*/V) = \alpha_{SF}6/D_V \tag{10}$$

For a more general case, the condition $A/V = \text{const}$ can be rewritten as:

$$A/V = \alpha_i/X_i = \text{const} \tag{10.1}$$

where X_i is any characteristic size, e.g., which is conveniently measured, and α_i is the adequate shape coefficient. This allows expression of the size of complex shapes through the size of spheres of equivalent volume, or surface area, through the size

of an inscribed or conscribed sphere, etc., through equivalents of another shape, namely polyhedral, cylindrical, or any other convenient shape.[57,58] It is important that the sizes measured on the basis of different equivalents are interrelated. For example, let us consider the particles and pores of an arbitrary closed shape, which have known volume V and surface area A. The values of A and V are expressed though the characteristic size X as[57]

$$A = k_A X^2 \text{ and } V = k_V X^3 \tag{11}$$

where k_A and k_V are shape factors, interrelated through the same values of X. In this case

$$A/V = \alpha_{AV,i}/X_{AV,i} = \alpha_{AV,j}/X_{AV,j} = \alpha_{AV,w}/X_{AV,w} = \alpha_i/d_i \tag{12}$$

where $\alpha_{AV,i} = k_{A,i}/k_{V,i}$ are the shape factors in system i, $\alpha_{AV,j}$ and $\alpha_{AV,w}$ are that in systems j and w. For example, the characteristic size X of particle can be expressed through the diameter of the sphere X_k with the equivalent surface-to-volume ratio, in this case $A/V = 6/X_k$; for a cylinder with the length H and diameter d_{Cyl} as an equivalent having the same V/A ratio, we obtain: for $H/d_{Cyl} \gg 1.0$ (long cylinder) $A/V = 4/d_{Cyl}$; for $H/d_{Cyl} \ll 1.0$ (disk) $A/V = 2/H_{Cyl}$, where H_{Cyl} is the thickness of the disk, etc. The flat disk can be transformed to a thin plate or an adsorbed layer, for which the surface area is equal to the surface area of adsorbent. In these cases, $A/V = 2/t$, where t is thickness of plate or layer, etc. Such analysis is equally applicable for particles, and pores. In all cases. the characteristic size can be expressed via the shape coefficient:

$$\alpha_i = (A/V)d_i \tag{12.1}$$

where values α_i and d_i are connected by ratios of the type of eq 12. In the considered cases, e.g., at the situation shown in Figure 2b, the values A and V for the host may be defined from adsorption experiments.

The earlier investigations devoted to the problem of the shape factors were intensively discussed in ref 58 (see also refs 57, 59), the recent works are cited in, e.g., ref 60. However, for this problem, the limits of eqs 1 and 4 using the ratio α/d determined by eqs 5 or 9 demands further study. In the experimental part of the current work, we applied the cylindrical approximation for silica gels pores and hydrate particles. In this case, $\alpha/d = A/V$, $\alpha = 4$, if d is the diameter of pores; A and V are the values of the specific surface area and pore volume of host (silica gel), correspondingly. Increase of anisotropy of the confined hydrate particles (e.g., Figure 2c) leads to the situation with $\alpha = 2$, as it was discussed above. In ref 61, we succeeded in choosing a method to determine the pore size for a mesoporous host for which the α values vary within the range from 2 to 4. This allowed us to carry out formal analysis of the effect of hydrate particle shape on the decomposition temperature of confined gas hydrate. In the present work, we describe new experimental data obtained within a broad pressure range for the equilibrium conditions of decomposition of the particles of methane, ethane, propane, and carbon dioxide gas hydrates dispersed in the confining mesopores of silica gel. On the basis of the obtained data, we discuss the effect of different factors on temperature of hydrate decomposition in the confinig pores.

Experimental Section

In our investigation, we used commercially available standard series of silica gel with a narrow Gauss-like mesopore size distribution: KSK-1, KSK-2, KSS-3, and KSS-4. The samples were crushed to the particle size of 0.05−0.1 mm, annealed in air at 400 °C to remove adsorbed species, then hydrated by boiling in water for 48 h, and dried at 200 °C. Samples of silica gel with the water content slightly less than 100% were used in experiments. The samples were prepared by exposure to the saturated water vapor over KOH solutions of different concentrations; the content of adsorbed water was measured on the basis of changes in the sample mass. The texture characteristics of all the samples were determined on the basis of nitrogen adsorption at 77 K with ASAP-2400 instrument (Micromeritics, USA). Pore sizes were calculated from nitrogen adsorption isotherms by the use of several methods (Table 1).

TABLE 1: Diameter of Mesopores in Silica Gels[a]

silica gel	mean pore size, d (nm), determined using different methods				
	d_{BET}	$d_{BJH,ads}$	$d_{BJH,des}$	$d_{max,ads}$	$d_{max,des}$
KSK-1	11.3	12.6	10.4	29.6 (11.8)	20.2 (9.3)
KSK-2	12.6	11.3	9.8	18.8 (9.2)	12.0 (2.7)
KSS-3	7.61	6.6	5.7	10.5 (6.3)	6.9 (1.3)
KSS-4	4.41	4.3	3.8	5.9 (4.1)	4.3 (1.0)

[a] Semiwidth values of Gaussian peak measured at the half-height of the plots of differential pore distribution over characteristic size (PSD) are given in parentheses.

The $d_{BET} = 4V_\Sigma/A_{BET}$ value was determined from the specific pore volume V_Σ, which was measured from the limiting saturation with nitrogen. The A_{BET} value, which is the specific surface area of silica gel, was calculated from the isotherm using the BET procedure.[62] Pore size distributions (PSD) were calculated using the standard Barret−Joiner−Halenda (BJH) procedure within the model of nonintersecting cylindrical pores[62] using the adsorption and desorption branches of nitrogen adsorption isotherms. The $d_{max,ads}$ and $d_{max,des}$ values correspond to the maxima of corresponding PSDs over the adsorption and desorption branches of isotherms, respectively. The $d_{BJH,ads}$ and $d_{BJH,des}$ values were determined as $4\Delta V_i/\Delta A_i$, where ΔV_i and ΔA_i are the increments of the pore volume and the surface area, calculated using the BJH procedure for the pores of different sizes. A more detailed discussion of these values is given in ref 61.

The temperatures of hydrate dissociation were measured by differential thermal analysis (DTA) under high pressures. The method of differential thermal analysis gives a maximum thermal effect at the temperature of hydrate dissociation in the predominant pores of the sample; the volume portion of the hydrate in these pores is maximum, and, hence, causes the maximal heat absorption. The monitored temperature of hydrate dissociation corresponds to the hydrate dissociation in such pores, and the scatter of pore size causes just a broadening of differential peak.[61] The experimental apparatus was described in detail elsewhere.[63] Samples of silica gel with adsorbed water were loaded into the DTA container with a volume of 0.05 mL. The container was hermetically assembled with a 6−8 mL stainless steel flask supplied with a movable piston and a back valve. After that, the flask was filled with methane gas at pressures up to 2 MPa. A special technique was used for loading of the experimental cell with the silica gel and gas, which allowed one to avoid changes in the water content in the sample of silica gel. The assembled cell was placed into the zone of high hydrostatic pressure produced by compression of a silicon oil−hexane mixture. The pressure was transmitted into the cell by means of the piston. Temperatures of phase transformations were recorded in a course of heating the DTA cell at the moment of maximal difference of temperatures between standard thermo-

couple and thermocouple introduced into the container with sample. Typical experimental series included 7−15 independent cycles of freezing−seasoning−annealing of the sample to reach equilibrium heating. The time of the seasoning procedure was varied from several minutes to 1−2 days. No significant trend in the hydrate decomposition temperatures was observed over this time scale.

Thermograms (sample temperature vs time and differential sample temperature vs time) were recorded at the last stage of the cycle. The appearance of peaks at the differential curve, which correspond to absorption of heat in the sample (will be referenced to below as thermal effects), evidenced a phase transformation taking place in the sample. In our case, thermal effects correspond to decomposition of all of the gas hydrate or some part of the gas hydrate in the sample. In the last case, several thermal effects corresponding to decomposition of different parts of gas hydrate in the sample occurred at the thermogram. The temperature of the sample measured at the moment of maximum peak at the differential curve corresponds to the decomposition temperature of the gas hydrate. In typical experiments, the decomposition points of the methane hydrates were measured with a chromel−alumel thermocouple in a standard DTA scheme with a heating rate of 1−2 °C/min. When calculating the *K* coefficients in eq 4, temperatures of hydrate dissociation under a given pressure were obtained by approximation of experimental data. The thermocouple was calibrated using reference points or a reference thermometer. The systematic error in measurement of temperature by thermocouple did not exceed 0.2 °C. The pressure was measured with Bourdon manometers (up to 250 MPa), calibrated using a load-piston manometer. At higher pressures, a Manganin manometer was used, which was calibrated via the melting point of mercury. The systematic errors of pressure measurements did not exceed 1% of the measured pressure value for pressures above 200 MPa (Manganin manometer, maximum error 10 MPa at pressure 1 GPa) and 0.5% of the measured pressure value for lower pressures (Bourdon gauge, maximum error 1 MPa at pressure 200 MPa). In our experiments, dissociation temperatures of gas hydrate were determined at a given pressure, and hence the maximum systematic error in determined dissociation temperatures includes a typical error of temperature measurement by DTA method and an error in decomposition temperature caused by the uncertainty in pressure. This value in our experiments does not exceed ±0.3 °C. Some examples illustrating correctness of the experimental procedure are given in ref 61. An example illustrating good agreement of our experimental data on methane hydrate obtained earlier with the use of the experimental procedure discussed above[61] with some data taken from literature is presented in Figure 3.

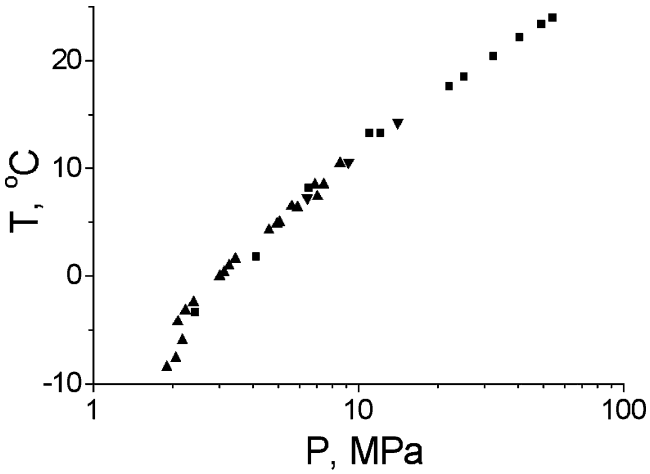

Figure 3. Comparison of our data[61] on decomposition temperatures for methane hydrate dispersed in the mesopores of silica gel KSK-1 with the pore size 29.6 nm (squares) with the data of ref 6 for mesoporous media with the pore size of 30 nm (up triangles) and the data of ref 7 for mesoporous media with the pore size of 30.6 nm (down triangles).

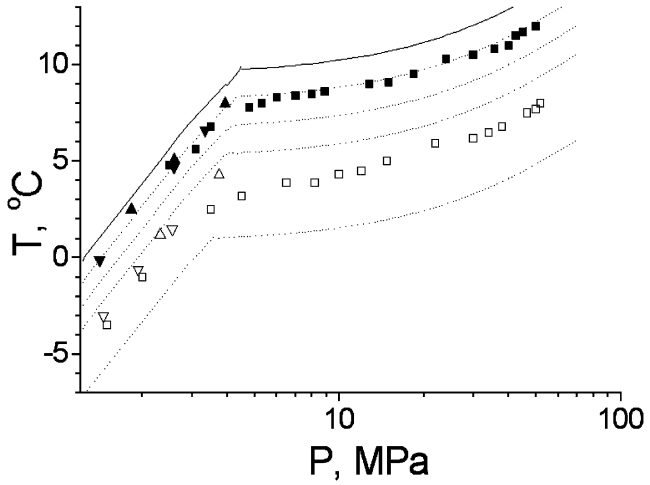

Figure 4. Experimental data on the decomposition of carbon dioxide hydrate dispersed in the pores of silica gel: (■) KSK-1 (29.6 nm); (□) KSS-3 (10.5 nm) in comparison with the calculated curves for the hydrate particle size of 28.6 and 9.5 nm, respectively. The size of hydrate particles is equal to the mean pore diameter minus the thickness of strongly bound water layer. The dashed curves (from top to bottom) were calculated assuming $\alpha = 2$ and particle size of 28.6 nm, $\alpha = 4$ and particle size of 28.6 nm, $\alpha = 2$ and particle size of 9.5 nm, $\alpha = 4$ and particle size of 9.5 nm. Solid line indicates the curve of decomposition of the bulk hydrate. Down triangles mark the data for comparison taken from ref 7 for mesoporous media with pore size 30.6 nm (solid triangles) and 9.2 nm (open triangles), up triangles mark the data from ref 6 for mesoporous media with pore size 30 nm (solid triangles) and 10 nm (open triangles).

Results and Discussion

Some experimental results corresponding to the decomposition of carbon dioxide, ethane, and propane hydrates dispersed in the pores of silica gels are shown in Figures 4−6. Unlike the previously investigated methane−water system,[61] in all systems concerned in the present work, the quadrupole point corresponding to the appearance of the phase of liquid guest in the respective systems can be found after achieving a definite pressure; a transition from "hydrate ↔ $(H_2O)_{liquid}$ + G_{gas}" to "hydrate ↔ $(H_2O)_{liquid}$ + G_{liquid}" decomposition scheme occurs. This is observed as a fracture of hydrate decomposition curves in phase diagrams. Interpretation of the obtained experimental results was carried out on the basis of Gibbs−Thomson eq 4. The results of the interpolation taking into account values listed in Table 2 are shown in Figures 4−6. The numerical data on the decomposition of bulk hydrates were taken from refs 1, 70−72. On the basis of the information reported in ref 61, the values of the *K* coefficient in eq 4 were accepted to be independent of pressure; they were calculated by accounting for the composition, unit cell parameters, and heat of decomposition for these hydrates. For *K* in the regions where G exists in a liquid state, we subtracted heat of evaporation of G from the heat of hydrate decomposition. Choice of the parameters necessary to calculate *K* was based on literature survey with selection of the most reliable data, with the preference to the values determined independently by different authors. Possible

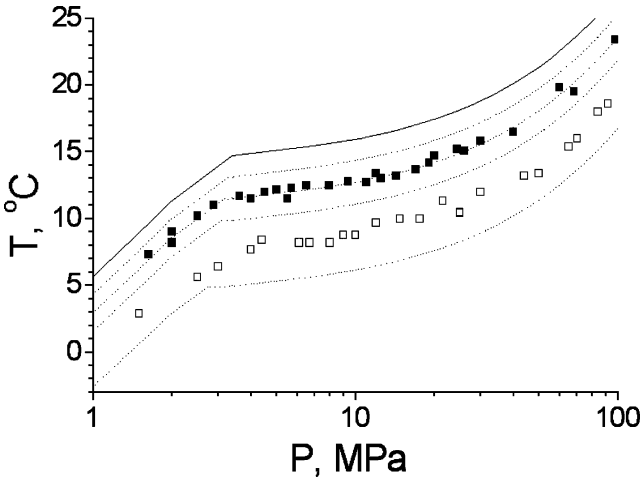

Figure 5. Experimental data on the decomposition of ethane hydrate dispersed in the pores of silica gel: (■) KSK-1 (29.6 nm), (□) KSS-3 (10.5 nm), in comparison with the calculated curves for the hydrate particle size of 28.6 and 9.5 nm, respectively. The size of hydrate particles is equal to the mean diameter of pores minus the thickness of strongly bound water layer. The dashed curves (from top to bottom) were calculated assuming $\alpha = 2$ and particle size of 28.6 nm, $\alpha = 4$ and particle size of 28.6 nm, $\alpha = 2$ and particle size of 9.5 nm, $\alpha = 4$ and particle size of 9.5 nm. Solid line indicates the curve of decomposition of the bulk hydrate.

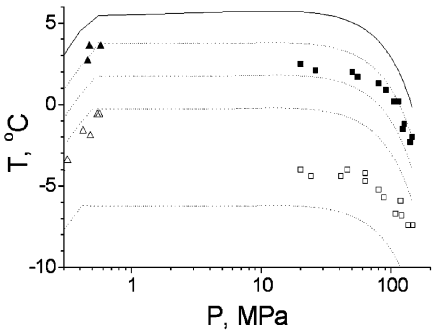

Figure 6. Experimental data on the decomposition of propane hydrate dispersed in the pores of silica gel: (■) KSK-1 (29.6 nm), (□) KSS-3 (10.5 nm) in comparison with the calculated curves for the hydrate particle size of 28.6 and 9.5 nm, respectively (the size of hydrate particles is equal to the mean pore diameter minus the thickness of strongly bound water layer). The dashed curves (from top to bottom) were calculated assuming $\alpha = 2$ and particle size of 28.6 nm, $\alpha = 4$ and particle size of 28.6 nm, $\alpha = 2$ and particle size of 9.5 nm, $\alpha = 4$ and particle size of 9.5 nm. Solid line indicates the curve of decomposition of the bulk hydrate. Up triangles mark the data from ref 6 for mesoporous media with pore size of 30 nm (solid symbols) and 10 nm (open symbols) shown for comparison.

changes in the equilibrium stoichiometry of the hydrates of carbon dioxide and ethane with the increase of pressure were not taken into account because of the absence of the corresponding data. The surface tension values for the interface between liquid water and hydrate were accepted to be equal to 0.029 J/m^2, similar to that for the interface between water and ice.[7,61] This assumption is based on the similarity of ice and the hydrates' molecular structures. The characteristic pore size was accepted to be equal to the above-considered value $d_{max,ads}$ diminished by 1 nm, which is an average statistical thickness of water films strongly bound to the surface and thus taking no part in hydrate formation.

Let us consider the pressure range up to 100 MPa first. One can see in Figures 2−4 that the experimental points always fall into the range limited by the calculated curves for $\alpha = 2$ and 4. This allows the assumption that a decrease in the temperature of hydrate decomposition in silica gel mesopores can be estimated using the eq 4 without any special fit for the parameters involved in this equation. The hydrates of methane[61] and CO_2 (Figure 4) in silica gels KSK-1 and KSK-2 with relatively large pores form particles with the experimental shape coefficient close to 2, which is formally evidence of deep and anisotropic "germination" of the hydrates into the pore space of the host and, consequently, significant shape anisotropy of the confined hydrate. The shape coefficient slightly increases with a decrease of pore size. This can be interpreted as the hindered "germination" of hydrates through the "windows" in the porous framework of a host that usually have smaller sizes compared to surrounding pores. As a result, each hydrate particle is ultimately localized in linear forms of the chains of filled cavities. In the case of CO_2 hydrate, good solubility of carbon dioxide in water promotes the formation of coarse hydrate particles occupying several adjacent cavities separated by rather broad "windows". In the case of ethane hydrate, an opposite situation is observed (Figure 5). In silica gel with large pores, hydrate particles with the shape coefficient close to 4 are formed; a decrease in pore size somewhat decreases the shape coefficient corresponding to the formation of aggregates composed of the hydrate particles. This was reproduced in independent experiments with ethane hydrate. Several sets of experiments with propane hydrate did not reveal any clear trend (Figure 6). It is known that, at high pressures, propane−water systems reach equilibrium much slower in comparison with other systems under consideration. This can explain low reproducibility of the experimental data. Similarly to methane hydrate,[61] the DTA thermograms often exhibited several neighboring heat effects in the systems under our consideration. Formally, this corresponds to the occurrence of several points of hydrate decomposition for the same sample. This effect can be explained by coexistence of the populations of hydrate particles with different sizes, which decompose at different temperatures. Another (less probable) interpretation may be related with variations of the γ_{SH} value.

The decomposition curves for ethane hydrate recorded under pressures above 100 MPa exhibit behavior rather similar to that observed under low pressures (Figure 7a). Within the whole pressure range investigated, the same ethane hydrate of cubic structure I exists in the system ethane−water.[70] The decomposition curves within this range are close to the curve calculated for $\alpha = 2$ and go even somewhat higher. A noticeable scattering of the points is observed along with the appearance of coupled effects. The behavior of hydrates formed in the propane−water system under high pressure are much more complicated (Figure 7b). Within the pressure range under consideration, three different propane hydrates can exist in the system at pressures up to 1.5 GPa.[71] The structure was determined only for the low-pressure hydrate (cubic structure II). In all of the experiments with propane, a noticeable difficulty in achieving of an equilibrium state was observed with pressure increase. For KSK-1 and KSK-2 silica gels, the curves of hydrate decomposition behave similarly. Both curves go lower than the curves of decomposition of the bulk hydrates; different ΔT is observed for different pressure. Formally, this observation can be linked with variations of the shape coefficient for hydrate particles α under different pressures. A more detailed consideration does not seem possible at this point. The behavior of propane hydrate dispersed in KSS-3 silica gel under pressure exceeding 400 MPa is principally different from the cases considered above. Two thermal effects are observed within the whole pressure range. ΔT for

TABLE 2: Pore-Size Dependent Parameters of Gibbs−Thomson Equation Used in Calculation of Lowering of Decomposition Temperature for Hydrates of Different Gases Dispersed in Silica Gel Mesopores[a]

G	hydrate composition	ΔH_h kJ/mol	ΔH_g kJ/mol	a_{cell} Å	v_h cm^3/mol	K nm
CH_4	$CH_4 \cdot 6H_2O$ [ref 1]	54.19 [ref 1]		12.02 [ref 1]	136.5	-7.30×10^{-11}[b]
C_2H_6	$C_2H_6 \cdot 7.67H_2O$ [refs 1, 64, 65]	71.80 [ref 1]	9.12 [ref 69]	12.03 [ref 1]	174.8	-8.09×10^{-11}[b]
						-7.06×10^{-11}[c]
C_3H_8	$C_3H_8 \cdot 17H_2O$ [ref 1]	129.2 [ref 1]	16.43 [ref 69]	17.40 [ref 1]	396.7	-10.20×10^{-11}[b]
						-8.91×10^{-11}[c]
CO_2	$CO_2 \cdot 6.2H_2O$ [refs 66, 67]	65.2 [ref 68]	10.32 [ref 69]	12.07 [ref 1]	138.6	-7.32×10^{-11}[b]
						-6.17×10^{-11}[c]

[a] G, hydrate-forming gas; ΔH_h, enthalpy of decomposition into $(H_2O)_{liquid} + G_{gas}$; ΔH_g, enthalpy of evaporation G at 0 °C; a_{cell}, the unit cell parameter of hydrate at 0 °C; v_h, the molar volume of hydrate; K, factor in eq 4. [b] Hydrate decomposition into $(H_2O)_{liquid} + G_{liquid}$ [c] Hydrate decomposition into $(H_2O)_{liquid} + G_{gas}$.

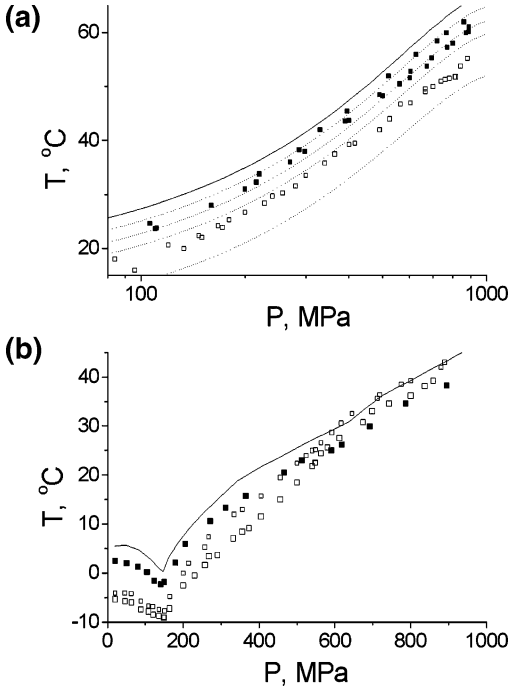

Figure 7. Experimental data on the high-pressure decomposition of ethane (a) and propane (b) hydrates dispersed in mesopores of (■) KSK-1 and (□) KSS-3 silica gels in comparison with the calculated curves for the hydrate particle size of 28.6 and 9.5 nm, respectively. The size of hydrate particles is equal to the mean pore diameter minus the thickness of strongly bound water layer. The dashed curves (from top to bottom) were calculated assuming $\alpha = 2$ and particle size of 28.6 nm, $\alpha = 4$ and particle size of 28.6 nm, $\alpha = 2$ and particle size of 9.5 nm, $\alpha = 4$ and particle size of 9.5 nm. Solid line indicates the curve of decomposition of the bulk hydrate.

the decomposition curve of propane hydrate decreases and the upper branch of the curve approaches the decomposition curve for the bulk hydrate. This observation was reproduced in three independent sets of experiments. We explain this observation by the formation of propane hydrate outside the porous space. Probably, the growth of hydrate particles occurs on the external surface of silica gel particles due to water transport from the internal porous space through the liquid films wetting the surface of mineral particles (see below).

It should be noted that the results of our calculations for mesoporous hosts in the majority of cases are in good agreement with the data available from literature[6,7] for the hosts with similar mesopore size (Figures 4, 6). Taking into account the dependence of the pore size on the calculation procedure (Table 1) and the fact that the values most often used in the literature are d_{BET} and $d_{BJH,ads}$ (with our designations), it may be assumed that the authors of refs 6, 7 carried out critical comparison of

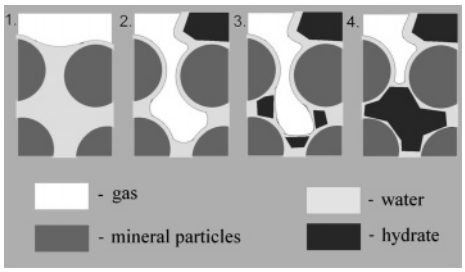

Figure 8. Scheme illustrating the growth of gas hydrate in the pore space of silica gel. For explanations, see the text.

different procedures of pore size calculation, although this question was not considered in the works themselves. The reasons for noticeable deviations that are observed in some cases between our data and those reported in the literature will be considered below.

Let us discuss a probable *qualitative* scenario of the formation of hydrate particles in the pore space of the host (Figure 8). This scenario can have somewhat speculative character because it is very difficult to carry out direct experimental investigation of the mechanisms of hydrate formation at present.

To begin with, a hydrate can be formed in the pore space only from the capillary condensate (see ref 61). Therefore, water film strongly bound to the host surface does not participate in the formation of hydrate. In our experiments, we used silica gel samples, the water content of which varied from the value corresponding to the initial point of the region of capillary condensation until complete saturation with water vapor, with the assumed limiting filling of pores with condensed liquid water. No noticeable systematic shift of the points with a decrease in water content was observed in this region (ref 61, the data of the present work). Then, it should be noted that it follows from the comparison between the stoichiometric molar volumes of the liquid water and of the hydrate that the hydrate volume is larger by about one-fourth than the volume of liquid water necessary for its formation. Thus, hydrate formation is accompanied by a noticeable increase in the volume of the condensed phase.

At the starting point, let the internal space of silica gel granules be completely filled with capillary-condensed water; the hydrate-forming gas is present between these granules (for example, their size is 0.05−0.1 mm) (Figure 8.1, initial state). At first, the nuclei of the hydrate phase should be formed near the boundary of three phases, gas−liquid−SiO_2, because the formation of a nucleus near the surface of mineral particles is favored by the heterogeneous nucleation mechanism. The formation at the gas−liquid boundary is promoted by the absence of difficulties with diffusion, e.g., of methane into the liquid-phase volume. The known data on the kinetics of hydrate

formation[1] show that, in the case of poor solubility of hydrate-forming gases, the formation of nuclei and growth of the hydrate occur near the surface of contact between the gas and water. This is evidence for the absence of any efficient mechanisms of gas transport inside the aqueous phase and especially through the solid hydrate. So, hydrate formation most probably starts near the *external* surface of the silica gel granules (Figure 8.2). In this case, the growth of hydrate particles is limited by the spaces between the host granules, but this size is out of the range of dimensional effects. In some experiments with an *excess* of liquid, we observed the effects corresponding to the formation of macroscopic bulk hydrate, which perfectly corresponds to the model under consideration. When only the internal pores of silica gel were filled with water, these effects were absent or did not manifest themselves due to their small value. In this case, the major part of hydrate particles was formed *inside* the pore space. This point is confirmed by the fact of existence of the dimensional effects. Because of this, we can pass to the second stage of the scenario. Now hydrate formation passes into the pores of the mesoporous host.

The above-mentioned decrease of the volume of the condensed phase accompanying the formation of hydrate and the growth of hydrate particles on the external surface should result in emptying of the pores near the growing hydrate particles. These pores can be filled with gas now, but water remains on their surface as an adsorbed film along which the transport to the growing crystal can proceed. The formation of nuclei of the new hydrate crystals in the volume of the matrix is at first prevented by the dependence of chemical potential on the size of hydrate particles, which conditions the so-called Ostwald ripening.[59,73] However, as the interface of water menisci goes deeper into the host volume and the length of water transport along the adsorption film increases, at a definite stage the nuclei starts formation within the host volume (Figure 8.3). At this stage, the growth of particles at the interface between gas and liquid is still possible due to water inflow from the inner regions of the porous space of the host particle (the outward growth). Partial mechanical pushing of the growing particle into the pore space cannot be excluded. The size and morphology of the growing hydrate particles can be affected by the solubility of gas, mobility of water in the adsorption film, detailed structure of the pore space of silica gel, etc. In addition, multiple repetition of the stages of formation of new nuclei is possible on the triple interface gas/solid/liquid moving into the silica gel volume. In any case, the geometric characteristics of the forming hydrate particles are to a large extent determined by the structure of the porous space of silica gel, which ensures manifestation of the corresponding dimensional effects during hydrate decomposition. The distribution of pores in silica gel on sizes and directions are almost noncorrelated, so for the growth of the hydrate into the depth, the characteristic mean size of hydrate particles corresponds to the mean pore size minus the thickness of the strongly bound water layer.

The assumed scenario of hydrate growth focuses on the effect of size and shape of particles on the experimentally measured temperature of decomposition of the hydrate dispersed in pores. The majority of experimentally observed features of the behavior of systems mesoporous host−hydrate−gas−water may be explained on the basis of the effect of these two factors. For example, for methane and carbon dioxide, which interact with pore water relatively fast, as suggested by our observations, our experimental data are in rather good agreement with the literature data (Figures 3, 4), while the curves of hydrate decomposition in these systems are close to the curves calculated for more stable particles with the surface curvature corresponding to $\alpha = 2$.

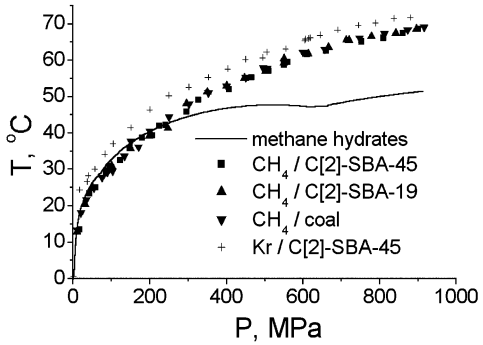

Figure 9. Decomposition curves for MeX and KrX. For explanations, see the text.

To conclude, we would like to present some results that give evidence of possible *increase* of decomposition temperature of the confined gas hydrates. These results are reliably reproducible and rather interesting in our opinion. We made an attempt to study the effect of the degree of hydrophobic power of the walls of the mesoporous host on the properties of hydrate confined in it (all the previous investigations were carried out with SiO_2-based hosts with hydrophilic walls). Investigations were carried out within a broad pressure range. At first, we investigated decomposition curves of methane hydrate dispersed in the mesoporous mesophase type of SBA-15 and carbon-coated SBA-15 (referred to as C−SBA-15-X, where X corresponds to the mass in percent of carbon in the material). Further investigation was carried out with various natural hosts, including charcoal and coal. Similar results were obtained in all the cases. At the first stage of our experiment, the compounds with decomposition points lying below (C−SBA-15-19 and C−SBA-15-45) or on the decomposition curve of the bulk methane hydrate (charcoal and coal) were formed. After long-term (2 weeks to 1 month) exposure of humid carbon sample under high (800−900 MPa) methane pressure, a compound was formed in the system, the decomposition curve of which was substantially different from that of the bulk methane hydrate and was going higher than the latter within a broad pressure range (Figure 9, this compound will be referred to as MeX). No effects were observed in blank experiments with the dry carbon matrix and dry gas. The curves of MeX decomposition, obtained for various carbon materials, did not exhibit noticeable differences, but the decomposition curve of the compound with krypton KrX (which was investigated for comparison) goes somewhat higher. These results show that, for the given pressure, the temperature of MeX decomposition is almost independent of the size (even existence) of mesopores in the carbon matrix; however, it depends on the nature of the gas involved. The nature of MeX remains unclear at present; however, on the basis of information mentioned in the Introduction, it may be assumed that the discovered phenomenon is connected with conglutination of hydrate particles with the hydrophobic walls of the host and is due to the related stabilization.

Acknowledgment. The investigation has been supported by the integration project of the SB RAS no. 147, by the Russian Foundation for Basic Research (project nos. 03-03-32020a, 04-03-32578a), by the Ministry of Science of the RF, project 2120.2003.3, and by the RAS program no. 13.3. A. Yu. Manakov thanks the Russian Science Support Foundation for financial support.

References and Notes

(1) Istomin, V. A.; Yakushev, V. S. *Gas Hydrates in Nature*; Moskow: Nedra, 1992 (in Russian).

(2) Melnikov, V. P.; Nesterov, A. N. *Earth's Cryosphere, Spec. Issue* **2003**, 76.

(3) Handa, Y. P.; Stupin, D. *J. Phys. Chem.* **1992**, *96*, 8599.

(4) Clennell, M. B.; Hovland, M.; Booth, J. S.; Henry, P.; Winters, W. J. *J. Geophys. Res. B* **1999**, *104*, 22985.

(5) Uchida, T.; Ebinuma, T.; Ishizaki, T. *J. Phys. Chem. B* **1999**, *103*, 3659.

(6) Uchida, T.; Ebinuma, T.; Takeya, S.; Nagao, J.; Narita, H. *J. Phys. Chem. B* **2002**, *106*, 820.

(7) Anderson, R.; Liamedo, M.; Tohidi, B.; Burgass, R. W. *J. Phys. Chem. B* **2003**, *107*, 3500, 3507.

(8) Smith, D. H.; Seshadri, K.; Uchida, T.; Widler, J. W. *AIChE J.* **2004** *501*, 589.

(9) Christenson, H. K. *J. Phys.: Condens. Matter* **2001**, *13*, R95.

(10) Alba-Simionesko, C.; Coasne, B.; Dudziak, G.; Gubbins, K. E.; Radhakrishnan, R.; Sliwanska-Barkowiak, M. J. *J. Phys.: Condens. Matter* **2006**, *18*, R15.

(11) Takagi, M. *J. Phys. Soc. Jpn.* **1954**, *9*, 359.

(12) Zhao, M.; Zhou, X. H.; Jiang, Q. *J. Mater. Res.* **2001**, *16*, 3304.

(13) Qi, W. H.; Wang, M. P. *Mater. Chem. Phys.* **2004**, *88*, 280.

(14) Jiang, Q.; Shi, M.; Zhao, M. *J. Chem. Phys.* **1999**, *111*, 2176.

(15) Faivre, C.; Bellet, D.; Dolino, G. *Eur. Phys. J. B* **1999**, *7*, 19.

(16) Goldstein, A. N.; Ether, C. M.; Alivisatos, A. P. *Science* **1992**, *256*, 1425.

(17) Smirnov, P.; Yamaguchi, T.; Kittaka, S.; Takahara, S.; Kuroda, Y. *J. Phys. Chem. B* **2000**, *104*, 5498.

(18) Janssen, A. H.; Talsma, H.; van Steenbergen, M. J.; de Long, K. P. *Langmuir* **2004**, *20*, 41.

(19) Koga, K.; Tanaka, H. *J. Chem. Phys.* **2005**, *122*, 104711.

(20) Loughnane, B. J.; Farrer, R. A.; Scodini, A.; Reilly, T.; Fourkas, J. T. *J. Phys. Chem. B* **2000**, *104*, 5421.

(21) Kanakubo, M.; Hiejima, Y.; Minami, K.; Aizawa, T.; Nanjo, H. *Chem. Commun.* **2006**, 1828.

(22) Thomson, J. J. *Application of Dynamics to Physics and Chemistry*; MacMillan and Co.: London, 1888.

(23) Pawlow, N. *Z. Phys. Chem.* **1909**, *65*, 545.

(24) Rie, E. *Z. Phys. Chem.* **1923**, *104*, 354.

(25) Batchlor, R. W.; Foster, A. G. *Trans. Faraday Soc.* **1944**, *40*, 300.

(26) Defay, R.; Prigogine, I.; Bellemans, A.; Everett, D. *Surface Tension and Adsorption*; Longmans, Green & Co.: London, 1966.

(27) Frenkel, J. *Kinetic Theory of Liquids*; Oxford University Press: Oxford, 1946.

(28) Reiss, H.; Wilson, I. B. *Colloid Sci.* **1948**, *3*, 551.

(29) Evans, R.; Marconi, U. *J. Chem Phys.* **1987**, *86*, 7138.

(30) Evans, R. *J. Phys.: Condens. Matter* **1990**, *2*, 8989.

(31) Brun, M.; Lallemand, A.; Quinson, J.-F.; Eyraud, C. *Thermochim. Acta* **1977**, *21*, 59.

(32) Quinson, J.-F.; Dumas, J.; Serughetti, J. *J Non-Cryst. Solids* **1986**, *79*, 397.

(33) Quinson, J.-F.; Dumas, J.; Chatelut, M.; Serughetti, J.; Guizard, C.; Larbot, A.; Cot, L. *J Non-Cryst. Solids* **1989**, *113*, 14.

(34) Denoyel, R.; Llewellyn, P.; Beurroies, I.; Rouquerol, J.; Rouquerol, F.; Luciani, L. In *Part. Part. Syst. Charact.* **2004**, *21*, 128.

(35) Yamamoto, T.; Endo, A.; Inagi, Y.; Ohmori, T.; Nakaiwa, M. *J. Colloid Interface Sci.* **2005**, *284*, 614.

(36) Gelb, L. D.; Gubbins, K. E.; Radhakrishnan, R.; Sliwanska-Barkowiak, M. *Rep. Prog. Phys.* **1999**, *62*, 1573.

(37) Radhakrishnan, R.; Gubbins, K. E.; Watanabe, A.; Kaneko, K. *J. Chem Phys.* **1999**, *111*, 9058.

(38) Kaneko, K.; Watanabe, A.; Iiyama, T.; Radhakrishnan, R.; Gubbins, K. E. *J. Phys Chem. B* **1999**, *103*, 7061.

(39) Radhakrishnan, R.; Gubbins, K. E.; Sliwanska-Barkowiak, M. *J. Chem. Phys.* **2002**, *116*, 1147.

(40) Nanda, K. K.; Sahu, S. N.; Behera, S. N. *Phys. Rev. A* **2002**, *66*, 13208.

(41) Warnock, J.; Awschalom, D. D.; Shafer, G. M. *Phys. Rev. Lett.* **1986**, *57*, 1753.

(42) Lutsco, J. F.; Wolf, D.; Philot, S. R.; Yip, S. *Phys. Rev. B* **1989**, *40*, 2841.

(43) Hakkinen, H.; Manninen, M. *Phys Rev. Lett.* **1992**, *55*, 1725.

(44) Nayak, S. N.; Khanna, S. N.; Rao, B. K.; Jena, P. *J. Phys.: Condens. Matter* **1998**, *10*, 10853.

(45) Evans, R.; Marini Bettolo Marconi, U.; Tarazona, P. *J. Chem. Soc., Faraday Trans. 2* **1986**, *82*, 1763.

(46) Seaton, N. A.; Walton, J. P.; Quirke, N. *Carbon* **1989**, *27*, 853.

(47) Malanoski, A. P.; van Swol, F. *Phys. Rev. E.* **2002**, *66*, 041602, 041603.

(48) Wallacher, D.; Künzner, N.; Kovalev, D.; Knorr, N.; Knorr, K. *Phys Rev. Lett.* **2004**, *92*, 195704.

(49) Sahimi, M. *Application of Percolation Theory*; Taylor & Francis: London, 1994.

(50) Deryaguin, B. V. *Acta Physicochem. USSR* **1940**, *12*, 181.

(51) Deryaguin, B. V.; Churaev, N. V.; Muller, V. M. *Surface Forces*: Consult Bureau: New York, 1987.

(52) Sklari, S.; Rahiala, H.; Stathopoulos, N.; Rosenholm, V.; Pomonis, P. *Microporous Mesoporous Mater.* **2001**, *49*, 1.

(53) Morishige, K.; Iwasaki, H. *Langmuir* **2003**, *19*, 2808.

(54) Engemann, S.; Reichert, H.; Dosch, H.; Bilgram, J.; Honkimäki, V.; Snigirev, A. *Phys. Rev. Lett.* **2004**, *92*, 205701.

(55) Guisbiers, G.; Wautelet, M. *Nanotechnology* **2006**, *17*, 2008.

(56) Sun, C. Q.; Li, C. M.; Bai, H. L.; Jiang, E. Y. *Nanotechnology* **2005**, *16*, 2005.

(57) Fenelonov, V. B.; Mel'gunov, M. S. Texturology. In *Surface and Nanomolecular Catalysis*; Richards, R., Ed.; Taylor & Francis, New York, 2006, pp 257−336.

(58) Allan, T. *Particle Size Measurement*, 3rd ed.; Chaptman and Hall: London, 1981.

(59) Fenelonov, V. B. *An Introduction to Physical Chemistry of the Formation of Supramolecular Structure of Adsorbents and Catalysts*, 2nd ed.; SB RAS Publications: Novosibirsk, 2004 (in Russian).

(60) Bouwman, A. M.; Bosma, J. C.; Vonk, P.; Wesselingh, J. A.; Frijlink, H. W. *Powder Technol.* **2004**, *146*, 66.

(61) Aladko, E. Ya.; Dyadin, Yu. A.; Fenelonov, V. B.; Larionov, E. G.; Mel'gunov, M. S.; Manakov, A. Yu.; Nesterov, A. N.; Zhurko, F. V. *J. Phys. Chem. B* **2004**, *108*, 16540.

(62) DeHoff, R. T., Phines, F. N., Eds. *Quantitative Microscopy*; McGraw−Hill Book Co.: New York, 1968.

(63) Dyadin, Yu. A.; Larionov, E. G.; Mirinskij, D. S.; Mikina, T. V.; Aladko, E. Ya.; Starostina, L. I. *J. Incl. Phenom.* **1997**, *28*, 271.

(64) Handa, Y. P. *J. Chem. Thermodyn.* **1986**, *18*, 915.

(65) Udachin, K. A.; Ratcliffe, C. I.; Ripmeester, J. A. In Proceedings of the Fourth International Conference on Gas Hydrates, Yokohama, May 19−23, 2002; p 604.

(66) Udachin, K. A.; Ratcliffe, C. I.; Ripmeester, J. A. *J. Phys. Chem. B* **2001**, *105*, 4200.

(67) Henning, R. W.; Schultz, A. J.; Thieu, V.; Halpern, Y. J. *J. Phys. Chem. A* **2000**, *104*, 5066.

(68) Kang, S. P.; Lee, H.; Ryu, B. J. *J. Chem. Thermodyn.* **2001**, *33*, 513.

(69) *Tables of Physical Parameters: A Handbook*; Kikoin, I. K.; Moscow: Atomizdat, 1976 (in Russian).

(70) Manakov, A. Yu.; Voronin, V. I.; Teplych, A. E.; Kurnosov, A. V.; Goryainov, S. V.; Ancharov, A. I.; Likchacheva, A. Yu. In Proceedings of the Fourth International Conference on Gas Hydrates, Yokohama, Japan, May 19−23, 2002; p 630−635.

(71) Dyadin, Yu. A.; Larionov, E. G.; Aladko, E. Ya.; Zhurko, F. V. *Dokl. Phys. Chem.* **2001**, *376*, 4−6, 23.

(72) Ng, H. J.; Robinson, D. B. *Fluid Phase Equilib.* **1985**, *21*, 145.

(73) Baldan, A. *J. Mater. Sci.* **2002**, *37*, 2171.